mathematics

MDPI

Article

Dynamic Mission Risk Management via Adaptive Information Acquisition and Online Uncertainty Calibration

Fanping Wei *, Yi Chen and Shihan Zhou

School of Reliability and Systems Engineering, Beihang University, Beijing 100191, China
* Correspondence: weifp@buaa.edu.cn

Abstract

Mission reliability and system survivability are jointly shaped by how risk management policies respond to evolving degradation and uncertainty in health information. Existing studies, however, predominantly rely on fixed information-acquisition schedules and pre-specified degradation trajectories, which limits the ability to adapt risk decisions to operating environments and heterogeneous degradation. This paper develops a dynamic mission risk management framework that integrates adaptive information acquisition with online uncertainty calibration. Specifically, the framework dynamically determines when additional degradation information should be acquired according to the current degradation state and mission progress, while sequentially updating uncertain degradation parameters through parameter learning. Under the specified random-effects Wiener model with exact observations, we establish that the latest degradation observation and its acquisition time are sufficient for Bayesian posterior updating. This property supports adaptive information acquisition, while intermediate observations remain valuable for timely risk assessment and intervention. A key insight is that the resulting optimal mission risk management policy admits a tractable threshold structure characterized by the system degradation level and mission progress. Exploiting these structural properties, an efficient solution algorithm is developed to streamline policy computation. Comparative experiments based on shipborne radar-driver degradation data demonstrate that the proposed framework consistently reduces risk-related losses relative to benchmark policies, highlighting the value of jointly adapting information acquisition and uncertainty calibration for dynamic mission risk management.

Keywords: mission reliability; risk control; mission abort; system survivability; uncertainty calibration

MSC: 90BXX

Check for updates

Academic Editor: Luigi Fortuna

Received: 31 August 2026
Revised: 9 October 2026
Accepted: 20 October 2026
Published: 26 October 2026

Copyright: © 2026 by the authors. Licensee MDPI, Basel, Switzerland. This article is an open access article distributed under the terms and conditions of the Creative Commons Attribution (CC BY) license.

1. Introduction

Mission-critical systems—extensively used in areas such as energy, aerospace, and rail transit—frequently confront the challenges of maintaining steady operations while preventing failures [1–3]. In recent decades, proactive measures tackling potentially severe risk-induced consequences of these systems have attracted increasing attention [4–8]. One of the most prevalent risk control measures undertaken in engineering practice is preventive maintenance. In particular, with the rapid advancement of sensor network technology and centralized data processing technologies, condition-based maintenance (CBM) empowered by real-time condition monitoring has become increasingly feasible [9–14]. However,

there are numerous industrial systems whose successful mission executions necessitate continuous operation without intervention, posing unique challenges for maintenance implementation, as mid-operation maintenance is almost impractical [15–20]. Such limitation has stimulated the adoption of mission abort strategies, an alternative methodology that evaluates mission completion risks against potential catastrophic system failures to minimize overall losses [21–24].

Since the seminal works initially presented by Myers, mission abort strategies have attracted increasing attention within the domains of operations research and risk management, with a series of inspiring practical applications [25]. Previous research on mission abort policies substantially falls into two categories from the perspective of system structure: single-unit abort policy and multi-unit abort policies [26–30]. The former focused primarily on single-machine-level systems with a unified abort framework, while the latter needs to first specify abort actions of distinct components and then optimize them jointly [31]. An extensive application of single-unit abort policies is on binary-state systems encountering either sudden failures or random shocks. In these works, the accumulated age or the number of shocks is commonly used as the risk criterion that determines whether to trigger abort actions [32].

Recent years have witnessed the advancement of sensor/inspection technology in evaluating degradation-based mission risks and informing condition-based mission abort decisions [33]. A typical application is on discrete multi-state systems, among which the most prevalent instance is three-state systems leveraging hidden defect as the abort criterion [34]. Similar studies have investigated mission abort policies utilizing early-warning signals under both constant and random mission durations [35]. For aging systems whose failure evolution can be averted through online interventions, the number of repairs guides condition-based abort decisions [36]. As for the risk control of continuously degrading systems, some researchers presented gamma processes to account for irreversible degradation, employing the monitored degradation level as the indicator for mission abort [37]. Follow-up works have developed abort strategies that integrate both degradation control limits and system age thresholds for mission abort determination [38]. Other studies have acknowledged the implications of imperfect state observation on abort model performance [39] and further developed computationally efficient algorithms to optimize mission abort models by balancing detection costs, mission costs, and failure costs under incomplete information [40].

Apart from single-component risk control models, there is also a growing interest in developing abort strategies managing integrated hazards of complex mission-critical systems. An intuitive means applicable to this class of problem is to view the number of failed components as key variables for mission termination [10]. Building upon this policy, a decision model oriented to multiple non-identical components was formulated to account for adaptive abort strategy [41]. Extended models have devised the joint optimization of routine planning and abort strategies for cooperative UAV systems [42], striving to balance mission reliability and system survivability by capturing the effects of failure propagation [43]. Other seminal works formulated the joint optimization problem of task assignment and selective abort among functional components [44]. Notably, most foregoing studies on mission abort utilized shock number or discrete states to describe the underlying system failure process [45,46], while risk control of continuous degradation processes powered by sensor technology is rarely reported, in particular for multi-component systems [47]. Stochastic processes such as Wiener, gamma, and inverse Gaussian are prevalent means to capture degradation dynamics in CBM models [48–51]. In contrast, only a handful of works have leveraged these processes to cope with degradation-centered mission termination

problems, while the implication of multiple uncertainties during degradation evolution is seldom reported [37].

Despite the rapid advancement of risk-aware mission abort methodologies, their application to heterogeneous aging systems confronts two fundamental challenges. Firstly, most existing abort models hinge exclusively on invariant inspection/monitoring policies to identify degradation severities [52]. While a periodic scheme is capable of reducing computational complexity, its rigid structure often leads to delayed failure detection or excessive inspection costs for systems with stochastic elements. Secondly, prevailing risk decision models are established based on a fundamental assumption of deterministic degradation pathways [53], which is increasingly being challenged due to multi-source uncertainties arising from manufacturing issues, operating conditions, and varying environments. To our knowledge, there is no systematic means that integrates adjustable information acquisition and parameter learning mechanisms to track the implications of heterogeneous degradation on mission risk control. Classical sequential analysis and optimal stopping theory have established fundamental principles for decision-making based on accumulating stochastic information [54,55]. Building upon these theoretical foundations, the present study focuses on a finite-horizon reliability optimization problem that jointly determines information-acquisition times and mission-abort decisions while updating uncertain degradation parameters.

This paper develops a dynamic mission risk management framework that integrates adaptive information acquisition with online uncertainty calibration. Unlike conventional mission abort models with pre-specified monitoring schedules and fixed degradation parameters, the proposed framework encodes the information acquisition process itself as an action into the decision space, and sequentially updates the uncertain deteriorating parameters. At each decision epoch, the decision-maker determines whether to continue or terminate the mission; conditional on continuation, the next information-acquisition epoch is also optimized. We establish a posterior sufficiency property under the specified degradation and observation assumptions: the latest degradation observation and its acquisition time are sufficient for updating the uncertain unit-specific drift. This property supports efficient Bayesian updating under irregular observations without implying that intermediate information acquisitions are unnecessary for timely risk intervention. We show that the optimal mission risk management policy admits a tractable dynamic control-limit structure. These structural properties are further exploited to reduce the decision space and enable efficient policy computation.

The main contributions and insights of this research can be summarized as follows: (a) **from a problem formulation perspective,** we formulate a dynamic mission risk management problem that jointly optimizes information acquisition and mission termination while continuously calibrating degradation uncertainty. We further establish a model-specific posterior sufficiency property that enables Bayesian updating from the latest exact observation and its acquisition time, while recognizing the role of intermediate observations in the timing of risk assessment and intervention; (b) **from a structure analysis perspective,** we characterize the optimal mission risk management policy through a dynamic control-limit structure. In particular, the threshold evolves with mission progress and responds systematically to the relative consequences of mission abort and system failure; (c) **from a management implication perspective**, we show that information acquisition should be treated as an endogenous risk-management decision rather than a fixed monitoring routine. By jointly optimizing acquisition and abort, decision-makers can reduce unnecessary monitoring while retaining timely risk intervention. Comparative experiments show that, compared to the baseline policy, this approach can significantly reduce risk-related losses.

The remainder of this research is structured as follows. Section 2 formulates the fundamental mission risk management problem bridging non-periodic information acquisition and parameter learning. Section 3 establishes the analytical properties of the optimal control policy. Section 4 demonstrates the model's applicability by comparison. Section 5 concludes with remarks and suggests potential avenues for future research.

2. Problem Formulation

We formulate an auto-updating risk control problem for a mission-critical system over a finite mission horizon. The key challenge is to balance mission reliability and system survivability under heterogeneous degradation while avoiding excessive information acquisition cost. Existing approaches mainly rely on fixed inspection schedules and static degradation assumptions, making them inadequate for jointly addressing decision flexibility, monitoring cost, and uncertainty in dynamic mission environments. To overcome this limitation, we develop an integrated framework that combines adaptive information acquisition with online uncertainty calibration. The framework enables operators to dynamically determine when to acquire health information according to the current degradation state and the remaining mission time. Under the specified random-effects Wiener model with exact observations, the framework supports efficient Bayesian updating from irregularly acquired degradation information using the latest observation and its acquisition time. Nevertheless, the timing of information acquisition remains important because it determines when updated degradation information becomes available for risk assessment and mission-abort decisions. As a result, it provides a unified means to achieve timely risk control, economical information acquisition, and robust uncertainty management throughout the mission.

2.1. Online Calibration of Degradation Uncertainty

Define $\{X(t), t \geq 0\}$ as a parametric stochastic process that describes the evolution of degradation during the mission. Without loss of generality, we characterize the degradation process by a generic transformed time scale term in conjunction with a Brownian error term. The transformed time scale $\Lambda(t;\boldsymbol{\theta}) = \int_0^t \boldsymbol{\theta}(u;\boldsymbol{\theta})du$ can take different forms, including but not limited to linear, exponential, or polynomial, which can flexibly adapt its trajectory pattern to endogenous system characteristics. Since $\boldsymbol{\theta}$ is the set of invariant parameters controlled by endogenous system characteristics, $\Lambda(t;\boldsymbol{\theta})$ is abbreviated as $\Lambda(t)$ afterwards. Consequently, the underlying degradation process is governed by $X(t) = v\Lambda(t) + \sigma B(\Lambda(t))$, where uncertain parameter v captures unit-to-unit heterogeneity, which affects system degradation trajectories through the form of an acceleration factor; $B(\cdot)$ represents Brownian motion with mean 0, and σ is the drift parameter. Figure 1 illustrates how adaptively acquired degradation observations support sequential parameter learning and mission risk decisions.

The uncertain unit-specific drift v can be sequentially updated through Bayesian inference as new degradation observations become available, with the resulting posterior variance quantifying the remaining parameter uncertainty. To this end, the prior distribution of v is assumed to be Gaussian with expectation μ and standard deviation κ. Then, parameter learning can be performed based on the joint set of information collection time $\mathbf{t} = \{t_1, t_2, \ldots, t_n\}$ and collected degradation level set $\mathbf{X} = \{X_1, X_2, \ldots, X_n\}$. The updated hyperparameters are denoted as $\langle\tilde{\mu}|\mathbf{X}, \mathbf{t}\rangle$ and $\langle\tilde{\kappa}|\mathbf{X}, \mathbf{t}\rangle$ and abbreviated as $\tilde{\mu}$ and $\tilde{\kappa}$.

The following assumptions underpin the parameter-learning derivation. The initial degradation level is known and set to $X(0) = 0$. The time transformation $\Lambda(t)$ is known, deterministic, and strictly increasing, with $\Lambda(0) = 0$, and the same transformation governs both the drift and Brownian terms. The diffusion coefficient σ is known and remains

constant during the mission. The unit-specific drift v is independent of the Brownian motion and remains unchanged throughout the mission; conditional on v, degradation increments over fixed, disjoint intervals are independent. The prior hyperparameters μ and κ are treated as fixed inputs. Degradation observations are exact, without measurement error, and each subsequent acquisition time is selected using only information already acquired.

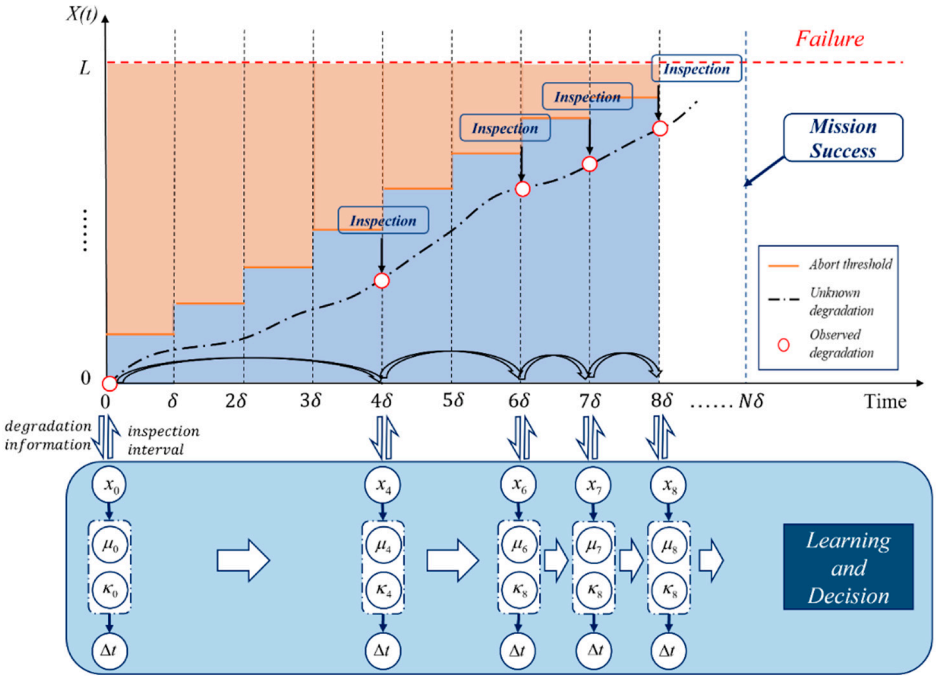


Figure 1. Schematic diagram of adaptive-observation-informed parameter learning and decision-making.

As previously stated, the prior density of drift v is $f_V(v|\mu,\kappa) = \frac{1}{\sqrt{2\pi\kappa^2}} \exp\left[-(v-\mu)^2/2\kappa^2\right]$. Also, the probability density of degradation severity with a known v is constructed as follows:

$$p(\mathbf{X},\mathbf{t}|v) = \prod_{i=1}^{n} \frac{1}{\sigma\sqrt{2\pi(\Lambda(t_i)-\Lambda(t_{i-1}))}} \exp\left\{-\frac{(X_i - X_{i-1} - v(\Lambda(t_i)-\Lambda(t_{i-1})))^2}{2\sigma^2(\Lambda(t_i)-\Lambda(t_{i-1}))}\right\}. \quad (1)$$

Accordingly, the posterior distribution density of v provided $\mathbf{X}$ and $\mathbf{t}$, yielding the following:

$$\begin{aligned} f(v|\mathbf{X},\mathbf{t}) &\propto f_V(v)p(\mathbf{X},\mathbf{t}|v) \\ &\propto \exp\left\{-\frac{1}{2}\left[\frac{(v-\mu)^2}{\kappa^2} + \sum_{i=1}^{n}\frac{(X_i - X_{i-1} - v(\Lambda(t_i)-\Lambda(t_{i-1})))^2}{\sigma^2(\Lambda(t_i)-\Lambda(t_{i-1}))}\right]\right\} \\ &\propto \exp\left\{\frac{v^2-2\mu v}{\kappa^2} + \sum_{i=1}^{n}\frac{v^2(\Lambda(t_i)-\Lambda(t_{i-1}))^2 - 2v(\Lambda(t_i)-\Lambda(t_{i-1}))(X_i - X_{i-1})}{\sigma^2(\Lambda(t_i)-\Lambda(t_{i-1}))}\right\} \\ &\propto \exp\left\{\frac{v^2-2\mu v}{\kappa^2} + \frac{v^2\Lambda(t_n) - 2vX_n}{\sigma^2}\right\} \propto \exp\left\{\frac{v^2 - 2v\frac{\mu\sigma^2+\kappa^2X_n}{\kappa^2\Lambda(t_n)+\sigma^2}}{\frac{\kappa^2\sigma^2}{\kappa^2\Lambda(t_n)+\sigma^2}}\right\}. \end{aligned} \quad (2)$$

Since the conjugate distribution is also Gaussian, it follows that the posterior distribution of drift v admits a Gaussian distribution with hyperparameters $\tilde{\mu}$ and $\tilde{\kappa}$, which can be formulated as follows:

$$\tilde{\mu} = \frac{\kappa^2 X_n + \mu\sigma^2}{\kappa^2\Lambda(t_n)+\sigma^2}; \tilde{\kappa}^2 = \frac{\sigma^2\kappa^2}{\kappa^2\Lambda(t_n)+\sigma^2}. \quad (3)$$

Under the assumptions stated above, Equation (3) shows that the posterior distribution of v depends on the observation history only through the latest observation X_n and its acquisition time t_n, together with the fixed prior and model parameters. This follows because the parameter-dependent terms in the increment likelihood involve $\sum_{i=1}^{n}[X_i - X_{i-1}] = X_n$ and $\sum_{i=1}^{n}[\Lambda(t_i) - \Lambda(t_{i-1})] = \Lambda(t_n)$. Consequently, X_n and t_n are sufficient for updating the posterior distribution of the unit-specific drift.

This sufficiency property implies that, when the final observation time and value are held fixed, omitting intermediate exact observations does not change the resulting posterior distribution of v. It therefore permits the observation history to be compressed into the current state and acquisition time for decision-making. However, this result does not imply that less frequent information acquisition preserves learning performance throughout the mission: intermediate observations provide earlier opportunities to update the posterior and intervene. Information-acquisition frequency thus remains important for the timing of risk assessment and mission-abort decisions.

Taken together, these results enable posterior updating and dynamic decision-making using a compact state representation under the stated model and observation assumptions. In particular, Equation (3) shows that the posterior variance of the unit-specific drift decreases as the transformed observation time increases, indicating a reduction in posterior uncertainty. However, this reduction does not guarantee a smaller estimation error for every realized degradation trajectory. Moreover, although intermediate exact observations can be omitted without changing the posterior distribution at a fixed final observation time and value, they remain valuable for providing earlier posterior updates and supporting timely mission-abort decisions.

Remark 1. *The sufficiency result is specific to the assumed degradation and observation models. With imperfect observations, for example $Y_i = X(t_i) + \varepsilon_i$, where the measurement errors are independent Gaussian variables with variance σ_ε^2 and are independent of the degradation process. The observed increments contain the terms $\varepsilon_i - \varepsilon_{i-1}$, which introduce dependence between adjacent increments. The latest noisy observation and its acquisition time are therefore generally insufficient for recovering the posterior distribution of v. Intermediate observations can provide additional information by helping distinguish latent degradation from measurement error, and parameter learning would require filtering based on the observation history or an equivalent recursively updated belief state. Likewise, if the diffusion coefficient or time-transformation parameters are uncertain, or the unit-specific drift varies during the mission, the present history-compression result need not hold. These extensions would require a richer learning model and decision state, and the acquisition-frequency trade-off would need to be reassessed.*

2.2. Auto-Updating Decision Model with Adaptive Information Acquisition

We focus on a safety-critical system that is responsible for continuously performing a mission of duration τ. During the entire mission process, the system experiences continuous degradation attributed to the combined effect of external environmental and endogenous degradation of components. As specified in Section 2.1, the inference of the degradation rate is progressively updated upon acquiring the latest degradation observation. Accordingly, managers can refine abort decisions dynamically by selecting from the action set $\mathcal{A}$, which involves the following:

- **Option A.** Continue the mission and collect the subsequent degradation information at $t^{'}$ $(t < t^{'} < \tau)$;
- **Option B.** Abort the mission instantly to guarantee system survivability at the cost of mission failure.

We adopt an inspection-epoch failure criterion. Following Liu et al. (2017) [56], a threshold crossing between inspections is not counted as a failure if the degradation indicator returns below L by the next inspection. The system is declared failed when its observed degradation level reaches or exceeds L at a scheduled inspection, including the mission endpoint. This criterion is appropriate for fluctuating condition indicators, such as vibration-based health measures, when a temporary threshold exceedance does not necessarily imply an irreversible loss of functionality. In this setting, L represents an unacceptable condition assessed at an inspection epoch, rather than a physical damage boundary whose first crossing necessarily causes permanent failure. Consequently, both the mission penalty loss c_m and system failure loss c_f are simultaneously incurred. If, however, the mission is decided to be terminated without failure involvement, only a penalty cost c_m is incurred. The cost of each inspection is c_i. To minimize the total risk-centered loss, we formulate the integrated problem of information acquisition and mission abort as a finite horizon Markov decision process.

Let $V(n,x)$ represent the minimal anticipated cost after performing degradation inspection at $n\delta$. For $n = 1,2,\ldots,N-1$ and $x < L$, the optimal value function can be expressed as follows:

$$V(n,x) = \min\{V(n,x,a), a \in \mathcal{A}\}, \tag{4}$$

Here, $V(n,x,0) \equiv c_m$ represents the expected cost of aborting the mission, and $V(n,x,a)$, $a > n$ represents the expected cost of continuing the mission, which is formulated as follows:

$$V(n,x,a) = c_i + \left(c_m + c_f\right) \cdot [1 - R(n,x,a)] + \int_{-\infty}^{L} V(a,x')f(x'|n,x,a)dx', \tag{5}$$

Here, $R(n,x,a)$ represents the conditional system reliability under state (n,x) and action a, (a,x') is the next state, and $f(x'|n,x,a)$ is the transition probability density. Notably, $V(n,x,a)$, $1 \le a \le n$ is an irrelevant term that can be removed during model formulation, which yields $V(n,x,a) \to \infty$, $1 \le a \le n$. Then, the transition density $f(x'|n,x,a)$ is formulated as follows:

$$f(x'|n,x,a) = \frac{\exp\left[-\frac{[x'-x-\tilde{\mu}(\Lambda(a\delta)-\Lambda(n\delta))]^2}{2\left[\tilde{\kappa}^2(\Lambda(a\delta)-\Lambda(n\delta))^2+\sigma^2(\Lambda(a\delta)-\Lambda(n\delta))\right]}\right]}{\sqrt{2\pi\left[\tilde{\kappa}^2(\Lambda(a\delta)-\Lambda(n\delta))^2+\sigma^2(\Lambda(a\delta)-\Lambda(n\delta))\right]}}. \tag{6}$$

Likewise, the conditional reliability $R(n,x,a)$ is given as follows:

$$R(n,x,a) = \Pr\{x' < L|n,x,a\} = \Phi\left(\frac{L-x-\tilde{\mu}(\Lambda(a\delta)-\Lambda(n\delta))}{\sqrt{\tilde{\kappa}^2(\Lambda(a\delta)-\Lambda(n\delta))^2+\sigma^2(\Lambda(a\delta)-\Lambda(n\delta))}}\right). \tag{7}$$

If the aging system survives through the catastrophic failure and no abort action is performed over the mission, then a reward c_r is obtained instantly. Then, the boundary equation at the N-th epoch is given as follows:

$$V(n,x|n=N) = \begin{cases} -c_r, & x < L, \\ c_m + c_f, & x \ge L. \end{cases} \tag{8}$$

The above iterative equation allows the optimal action to be sequentially determined leveraging a dynamic programming approach, and thereby the optimal mission execution policy can be established dynamically.

Figure 2 shows the realization flowchart of the established strategy. However, the calculation of the above iterative equations often encounters the challenge of state explosion. In particular, the decision space of the model developed in this paper is much larger than that of the traditional dual-action mission abort decision model, and the efficiency of the traditional value iteration algorithm plummets. Therefore, it becomes imperative to delve

deeper into the inherent structural features of the mission termination model to streamline the computational requirements, as we will specify in Section 3.

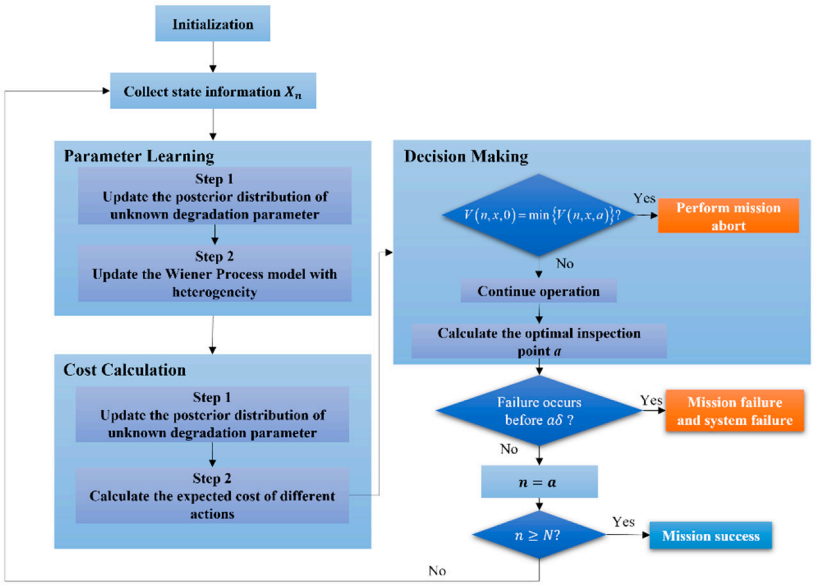


Figure 2. Flowchart of the joint framework for irregular inspection and abort decision.

3. Structural Properties

This section investigates the structural properties of the optimal decision model, and accordingly proposes algorithmic improvements to reduce the computational complexity. We theoretically establish the monotonicity of the value function, which serves as a fundamental pillar for the verification of the existence of control limits for mission abort. These properties promote the understanding of dynamic risk control decisions, which facilitates robust decision-making and time-efficient analytical computation. To begin with, we introduce the fundamental definition of the following stochastic order.

Definition 1. *A stochastic variable X is said to be stochastically smaller than a stochastic variable Y in the stochastic order, denoted by $X \prec Y$, if* $\Pr\{X \leq z\} \geq \Pr\{Y \leq z\}$ $\forall z$.

The utilization of Definition 1 allows us to explore the statistical behaviors of degradation increment under heterogeneity, as will be shown in Proposition 1.

Proposition 1. *For any pre-specified action $a \in \mathcal{A}$ and $\Lambda(t)$ with arbitrary concave–convex characteristics, the variable $\langle X_a|X_n\rangle$ is stochastically non-decreasing in X_n; in other words, $\langle X_a|X_n = x\rangle \prec \langle X_a|X_n = x^+\rangle$ provided $x < x^+$.*

Proof. The conditional distribution of v can be obtained as $\langle v|\mathbf{X}, \mathbf{t}\rangle \sim N(\tilde{\mu}, \tilde{\kappa}^2)$. According to Equation (3), $\tilde{\mu}$ is an increasing function of X_n, and $\tilde{\kappa}^2$ is constant in X_n. For $\forall x_1 \geq x_2$ and $\forall z \geq 0$, the following is established:

$$\Pr\{v \leq z|X_n = x_1\} = \Phi\left(\frac{z - \frac{\kappa^2 x_1 + \mu\sigma^2}{\kappa^2\Lambda(n\delta)+\sigma^2}}{\sqrt{\frac{\sigma^2\kappa^2}{\kappa^2\Lambda(n\delta)+\sigma^2}}}\right) \leq \Phi\left(\frac{z - \frac{\kappa^2 x_2 + \mu\sigma^2}{\kappa^2\Lambda(n\delta)+\sigma^2}}{\sqrt{\frac{\sigma^2\kappa^2}{\kappa^2\Lambda(n\delta)+\sigma^2}}}\right) = \Pr\{v \leq z|X_n = x_2\}. \quad (9)$$

It follows that $\langle v|X_n = x^+\rangle \succ \langle v|X_n = x\rangle$. Then, for $\forall v^1 \geq v^2$ and $\forall z \geq 0$, the following is established:

$$\begin{aligned}\Pr\{X_a - X_n \leq z|v^1\} &= \Phi\left(\frac{z-v^1(\Lambda(a\delta)-\Lambda(n\delta))}{\sigma\sqrt{\Lambda(a\delta)-\Lambda(n\delta)}}\right) \leq \Phi\left(\frac{z-v^2(\Lambda(a\delta)-\Lambda(n\delta))}{\sigma\sqrt{\Lambda(a\delta)-\Lambda(n\delta)}}\right) \\ &= \Pr\{X_a - X_n \leq z|v^2\}.\end{aligned} \tag{10}$$

It can be obtained that $\langle X_a - X_n|v^1\rangle \succ \langle X_a - X_n|v^2\rangle$. Thus, $\langle X_a - X_n|X_n = x^+\rangle \succ \langle X_a - X_n|X_n = x\rangle$, and, in turn, the following inequality is established:

$$\begin{aligned}\langle X_a|X_n = x^+\rangle &= \langle X_a - X_n|X_n = x^+\rangle + x^+ \\ &\succ \langle X_a - X_n|X_n = x^+\rangle + x \\ &\succ \langle X_a - X_n|X_n = x\rangle + x \\ &= \langle X_a|X_n = x\rangle.\end{aligned} \tag{11}$$

This closes the proof process. □

Proposition 1 establishes stochastic monotonicity of the predictive next-state distribution with respect to the current degradation level for a fixed decision epoch and continuation action. Proposition 2 uses this ordering to establish state monotonicity of the continuation and optimal value functions. Proposition 3 characterizes their sensitivity to information-acquisition cost. No general monotonicity with respect to the decision epoch is asserted.

Proposition 2. *Under the nonnegative cost parameters c_i,c_m,c_f,c_r, the continuation value $V(n, x, a)$ is non-decreasing in $x < L$ for every decision epoch $n < N$ and feasible continuation action $a \in A_n^+$. The optimal value $V(n, x)$ is also non-decreasing in $x < L$.*

Proof. For each subsequent epoch a, define the extended value function as follows:

$$\overline{V}_a(y) = \begin{cases} V(a, y), & y < L, \\ c_m + c_f, & y \geq L. \end{cases} \tag{12}$$

At the terminal epoch, $V(N, y) = -c_r$ for $y < L$. Since $-c_r \leq c_m + c_f$, the extended terminal value function is non-decreasing.

Suppose that $V(a, y)$ is non-decreasing on $y < L$ for all $a > n$. Immediate abort is feasible at each nonterminal epoch, so $V(a, y) \leq c_m$; the same bound holds at the terminal epoch because $-c_r \leq c_m$. Consequently, extending the value to $c_m + c_f$ on $y \geq L$ preserves monotonicity.

Let $Y_{n,x,a}$ denote the predictive degradation at epoch a. By Proposition 1, for $x \leq x' < L$, the following is established:

$$Y_{n,x,a} \leq_{\text{st}} Y_{n,x',a} \tag{13}$$

Since V_a is non-decreasing, Equation (5) gives the following:

$$\begin{aligned} V(n, x, a) &= c_i + \mathbb{E}\left[\overline{V}_a(Y_{n,x,a})\right] \\ &\leq c_i + \mathbb{E}\left[\overline{V}_a(Y_{n,x',a})\right] \\ &= V(n, x', a). \end{aligned} \tag{14}$$

Thus, each continuation value is non-decreasing in the current degradation level. The feasible continuation action set is independent of x, and the abort value c_m is constant. Therefore, the following applies:

$$V(n, x) = \min\{c_m, \min_{a \in A_n^+} V(n, x, a)\} \tag{15}$$

This is also non-decreasing in x. Backward induction completes the proof. □

Proposition 2 establishes that, at a fixed decision epoch, both the continuation value for each feasible action and the optimal value are non-decreasing in the current degradation level. The optimal value is bounded above by the immediate-abort cost c_m and equals c_m wherever abort is optimal. This state monotonicity supports the threshold characterization in Theorem 1 and permits higher degradation states to be assigned the abort action once abort is optimal at a lower state within the same epoch.

Proposition 3. *Fix a nonfailed state (n, x), the degradation model, and all cost parameters except the information-acquisition cost. Write $V_c(n, x)$ and $V_c(n, x, a)$ for the optimal and continuation values when $c_i = c$.*

(i) Both $V_c(n, x)$ and, for every fixed $a \in A_n^+$, $V_c(n, x, a)$ are non-decreasing and concave in $c \geq 0$.
(Ii) For $0 \leq c_1 < c_2$, let π_1 and π_2 be optimal policies at the corresponding acquisition costs. Their expected numbers of future acquisitions satisfy $E_{\pi_2}[N_I|n, x] \leq E_{\pi_1}[N_I|n, x]$.
(iii) At any interior value of cwhere $V_c(n, x)$ is differentiable, $\frac{\partial V_c(n,x)}{\partial c} = E_{\pi_c}[N_I|n, x]$ for any optimal policy π_c.

Proof. Let Π_n denote the set of admissible policies starting from (n, x). This set does not depend on the acquisition price. For a fixed policy π, define the following:

$$I_\pi(n,x) = E_\pi[N_I|n,x]. \tag{16}$$

and

$$B_\pi(n,x) = c_m \Pr_\pi(\mathcal{A} \mid n,x) + (c_m + c_f)\Pr_\pi(\mathcal{F} \mid n,x) - c_r \Pr_\pi(\mathcal{S} \mid n,x). \tag{17}$$

Here, $\mathcal{A}$, $\mathcal{F}$, and $\mathcal{S}$ denote mission abort, system failure, and mission success, respectively. The expected cost under this fixed policy is as follows:

$$J_\pi(n,x;c) = cI_\pi(n,x) + B_\pi(n,x). \tag{18}$$

Since $0 \leq I_\pi \leq N - n$, $J_\pi(c)$ is a non-decreasing affine function of c. Consequently, the following is established:

$$V_c(n,x) = \inf_{\pi \in \Pi_n} \{cI_\pi(n,x) + B_\pi(n,x)\}. \tag{19}$$

This is non-decreasing and concave. The same argument applies to $V_c(n, x, a)$ by restricting attention to policies whose first continuation action is a.

For part (ii), optimality at the two acquisition prices gives the following:

$$\begin{aligned} c_1 I_{\pi_1}(n,x) + B_{\pi_1}(n,x) &\leq c_1 I_{\pi_2}(n,x) + B_{\pi_2}(n,x) \\ c_2 I_{\pi_2}(n,x) + B_{\pi_2}(n,x) &\leq c_2 I_{\pi_1}(n,x) + B_{\pi_1}(n,x) \end{aligned} \tag{20}$$

Adding these inequalities yields the following:

$$(c_2 - c_1)\left[I_{\pi_2}(n,x) - I_{\pi_1}(n,x)\right] \leq 0. \tag{21}$$

This establishes the claimed ordering.

Finally, for an optimal policy π_c, the following applies:

$$V_{c+h}(n,x) \leq J_{\pi_c}(c+h) = V_c(n,x) + hI_{\pi_c}. \tag{22}$$

Using positive and negative h, and taking limits at a differentiability point, gives the following:

$$\frac{\partial V_c(n,x)}{\partial c} = I_{\pi_c}(n,x). \tag{23}$$

This completes the proof. □

Proposition 3 characterizes the economic adjustment of information-acquisition effort. As acquisition becomes more expensive, the optimal policy uses a weakly smaller expected number of future acquisitions. The concavity of the value function further indicates that its marginal sensitivity to acquisition price decreases as the policy adjusts its acquisition and abort decisions. At differentiability points, this sensitivity is exactly the expected number of future acquisitions, providing a direct link between the cost function and monitoring effort. The result concerns expected acquisition counts over the remaining mission; it does not require every state-specific acquisition interval to increase. A reduction in acquisition counts may result from longer intervals, earlier mission abort, or both.

We next characterize the abort region and derive computable bounds using the posterior predictive distribution. For $a \in A_n^+$, define $D_n = \kappa^2\Lambda(n\delta) + \sigma^2$, $d_{n,a} = \Lambda(a\delta) - \Lambda(n\delta)$ and $A_{n,a} = 1 + \frac{\kappa^2 d_{n,a}}{D_n}$, $B_{n,a} = \frac{\mu\sigma^2 d_{n,a}}{D_n}$, $s_{n,a} = \sqrt{\frac{\sigma^2\kappa^2 d_{n,a}^2}{D_n} + \sigma^2 d_{n,a}}$. The conditional next-state distribution is therefore $X(a\delta) \mid (n,x) \sim \mathcal{N}\big(A_{n,a}x + B_{n,a}, s_{n,a}^2\big)$ and $R(n,x,a) = \Phi\Big(\frac{L - A_{n,a}x - B_{n,a}}{s_{n,a}}\Big)$. For $0 < c_i + c_f$ and $c_i < c_m + c_r$, let $p^* = \frac{c_i + c_f}{c_m + c_f + c_r} \in (0,1)$, $b_{n,a} = \frac{L - B_{n,a} - s_{n,a}\Phi^{-1}(p^*)}{A_{n,a}}$, and $\overline{b}_n = \max_{a \in \{n+1,\ldots,N\}} b_{n,a}$.

Theorem 1. *For every decision epoch $n \in \{0,\ldots,N-1\}$, the following statements hold.*

(i) The optimal abort region is an upper interval of the nonfailed state space $x < L$. Define $C_n(x) = \min_{a \in A_n^+} V(n,x,a)$, $\mathcal{B}_n = \{x < L : C_n(x) \geq c_m\}$.

There exists a generalized threshold $\xi(n)$ such that mission abort is optimal if and only if $x \geq \xi(n)$, for $x < L$. We use $\xi(n) = L$ when $\mathcal{B}_n$ is empty and $\xi(n) = -\infty$ when all nonfailed states belong to the abort region.

(ii) If $0 < c_i + c_f$ and $c_i < c_m + c_r$, the threshold satisfies $\min\{L, b_{n,N}\} \leq \xi_n \leq \min\{L, \overline{b}_n\}$.

In particular, continuation is strictly preferred whenever $x < b_{nN}$, while abort is optimal whenever $b_n \leq x < L$. If $b_n < L$, a finite threshold strictly below L exists.

(iii) If $c_i \geq c_m + c_r$, immediate mission abort is optimal at every nonfailed state.

(iv) Under the conditions of part (ii), if $b_{n,N} \geq L$, continuation is strictly preferred to immediate abort at every nonfailed state, and $\xi_n = L$. Furthermore, if $c_i = c_f = 0$ and $c_m + c_r > 0$, continuation is strictly preferred at every nonfailed state and every decision epoch.

Proof. By Proposition 2, $V(n,x,a)$ is non-decreasing in x for every feasible continuation action. Since the action set is independent of x, $C_n(x)$ is also non-decreasing. Thus, if $x \in \mathcal{B}_n$ and $x \leq y < L$, then the following applies:

$$C_n(y) \geq C_n(x) \geq c_m, \tag{24}$$

Therefore, $y \in \mathcal{B}_n$.

For completeness, $C_n(x)$ is continuous on $x < L$. The extended subsequent value functions are bounded, and their expectations under the Gaussian predictive distribution are continuous in its mean, which is affine in x. A minimum over the finite continuation action set preserves continuity. Hence, a finite boundary within the nonfailed state space belongs to the abort region under the stated tie-breaking rule. This proves part (i).

To establish part (ii), observe that every subsequent value at a nonfailed state is bounded below by $-c_r$: future costs are nonnegative, and the mission-success reward is received at most once. Therefore, the following is established:

$$V(n,x,a) \geq c_i + (c_m + c_f)[1 - R(n,x,a)] - c_r R(n,x,a) = c_i + c_m + c_f - (c_m + c_f + c_r)R(n,x,a). \tag{25}$$

If $x \geq b_{na}$, the predictive probability satisfies $R(n, x, a) \leq p_*$, and this lower bound is at least c_m. Consequently, if $x \geq b_n$, every continuation action has a value at least c_m, and abort is optimal.

For the action $a = N$, the subsequent nonfailed value is exactly $-c_r$. Thus, the following applies:

$$V(n,x,N) = c_i + c_m + c_f - (c_m + c_f + c_r)R(n,x,N). \tag{26}$$

When $x < b_{nN}$, $R(n, x, N) > p_*$, so $V(n, x, N) < c_m$. Since this action is feasible, immediate abort cannot be optimal. These two certified regions establish the threshold bounds, with truncation at L representing the case of always continuing over the nonfailed state space.

If $b_n < L$, both a nonempty continuation region and a nonempty abort region exist. Moreover, b_{nN} is finite, so the threshold is finite and strictly below L.

Finally, any policy that starts with continuation incurs at least one acquisition cost and has subsequent total cost bounded below by $-c_r$. If $c_i \geq c_m + c_r$, its expected cost is therefore at least as follows:

$$c_i - c_r \geq c_m. \tag{27}$$

Immediate abort is optimal under the stated tie-breaking rule, proving part (iii).

To prove part (iv), suppose first that the conditions of part (ii) hold and $b_{n,N} \geq L$. Every nonfailed state satisfies $x < L \leq b_{n,N}$, and therefore $R(n, x, N) > p^*$. Consequently, $V(n, x, N) < c_m$, so immediate abort is strictly suboptimal throughout the nonfailed state space.

If $c_i = c_f = 0$ and $c_m + c_r > 0$, the value of continuing directly to mission completion becomes the following:

$$V(n,x,N) = c_m - (c_m + c_r)R(n,x,N) < c_m, \tag{28}$$

This is because the nondegenerate Gaussian predictive distribution gives $R(n, x, N) > 0$ for every finite $x < L$. Since this action is feasible at every decision epoch before mission completion, continuation is strictly preferred to immediate abort at every nonfailed state. This proves part (iv). □

Theorem 1 provides a threshold characterization together with explicit bounds that incorporate the current posterior predictive distribution. The lower boundary b_{nN} is obtained by considering direct continuation to the mission endpoint. Below this boundary, this feasible action already has a lower expected cost than immediate abort. The upper boundary b_n identifies states where every continuation action remains unattractive even when its subsequent nonfailed value is replaced by the most favorable bound $-c_r$. The condition $b_n < L$ therefore establishes a finite interior threshold without assuming that the next-inspection failure probability approaches one as the current state approaches L. Figure 3 illustrates the three possible mission outcomes under the threshold policy: mission success, mission abort, and system failure.

The bounds also support computational reduction. States satisfying $b_n \leq x < L$ can be assigned the abort action without evaluating all continuation alternatives. For states below b_{nN}, the immediate abort can be excluded, while the acquisition action is still optimized. Only the interval between the certified boundaries requires identification of the abort switching point. The bounds can be computed before backward induction using the posterior parameters and the feasible acquisition times. Their width indicates the remaining uncertainty about the switching location and may vary across decision epochs; no general temporal ordering of the optimal thresholds is imposed.

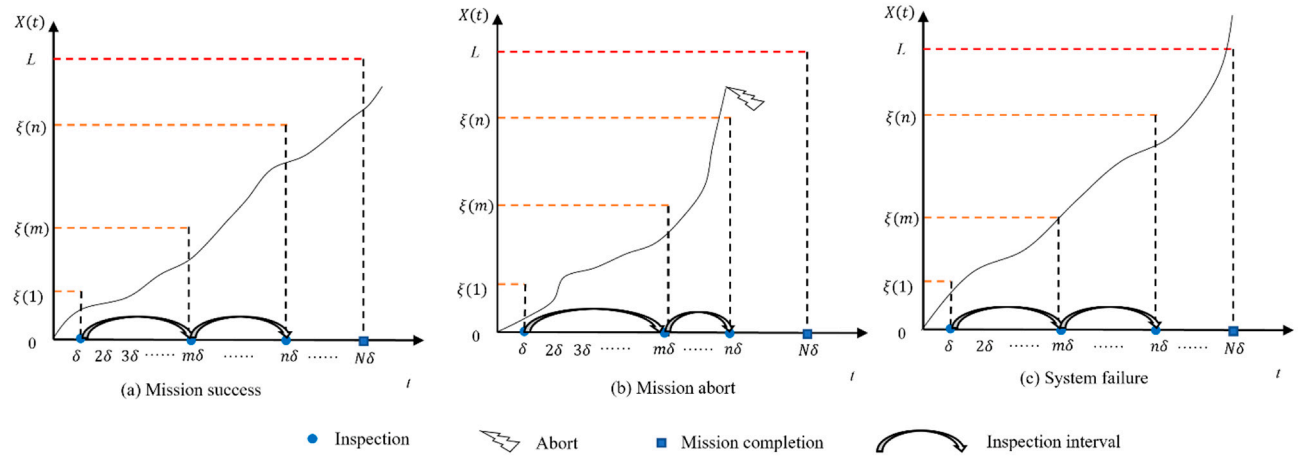


Figure 3. Schematic diagram of system degradation and risk control. (**a**) Mission success: the degradation trajectory remains within acceptable bounds and the mission is completed at the predetermined time. (**b**) Mission abort: the degradation level triggers an early abort decision before reaching the failure threshold. (**c**) System failure: the degradation trajectory exceeds the catastrophic failure limit L, resulting in system failure.

Remark 2. *Theorem 1 distinguishes the threshold structure from the existence of a finite, nondegenerate threshold. Monotonicity of the continuation value establishes that the abort region is an upper interval, but does not alone ensure that this region is nonempty. Under the conditions of part (ii), the additional condition* $b_n < L$ *guarantees both a nonempty continuation region at sufficiently low degradation levels and a nonempty abort region near the failure threshold. This condition is sufficient rather than necessary; a finite threshold may still exist when it is not satisfied. Parts (iii) and (iv) explicitly identify parameter conditions producing the degenerate policies of always aborting and always continuing, respectively. Thus, the existence of an interior abort threshold is treated as a conditional result rather than a universal feature of the model.*

Corollary 1. *The mission risk control limit* $\xi(n)$ *exhibits a non-increasing relationship with system failure cost* c_f *and a non-decreasing relationship with mission failure cost* c_m*.*

Proof. Set $\xi^1(n)$ and $\xi^2(n)$ as the control limits under system failure costs $c_m^1 < c_m^2$, respectively. Then, for any value function $V(n,x,a)$, $\forall a > n$, $\forall x > \xi^1(n)$, the following applies:

$$\begin{aligned} V\left(n,x,a\middle|c_f^2\right) &= c_i + \left(c_f^2 + c_m\right) \cdot [1 - R(n,x,a)] + \int_x^L V\left(a,x'\middle|c_f^2\right) f(x'|n,x,a)dx' \\ &> c_i + \left(c_f^1 + c_m\right) \cdot [1 - R(n,x,a)] + \int_x^L V\left(a,x'\middle|c_f^1\right) f(x'|n,x,a)dx' \\ &= V\left(n,x,a\middle|c_f^1\right) \\ &> c_m. \end{aligned} \tag{29}$$

Therefore, for $\forall x > \xi^1(n)$, $x > \xi^2(n)$ and $\xi^1(n) \geq \xi^2(n)$ are yielded. Hence, $\xi(n)$ is non-increasing in the failure cost c_f. Using a similar approach, the non-decreasing property of $\xi(n)$ with c_m is tractable. □

Corollary 1 discloses the monotonic nature of the risk control limit with respect to the economic parameters. In situations where system failure poses substantial costs, it becomes essential to maintain system survival. Consequently, the control limit should be set at a relatively low level to minimize the risk of potential failures. Conversely, when the economic consequences of mission abort are significant, the primary objective is to ensure mission completion. To maximize the probability of mission success, it is preferable to allow abort at a higher degradation level, thus increasing the likelihood of achieving mission objectives.

Based on the demonstrated structural properties, we present an improved backward induction algorithm to derive the optimal solution within a streamlined state space, which reduces computational resources substantially, **as detailed in Algorithm 1**.

Algorithm 1: Improved backward induction algorithm to find the optimal policy.

Input: Prior parameters μ,κ; diffusion coefficient σ; time transformation Λ; failure threshold L; costs c_m,c_f,c_i,c_r; decision interval Δ; terminal epoch N; grid boundary $x_{\min}$ and spacing Δ.
Output: Approximate values $\hat{V}$, grid actions O, and estimates or brackets for the abort thresholds.
Construct $x_j = x_{\min} + j\Delta$, $j = 0,\ldots,M$, with $x_M = L$
Interpret x_M as an auxiliary nonfailed left-limit node
Initialize $\hat{V}\left(N, x_j\right) = -c_r$ for all j using Equation (8).
For $n = N-1,\ldots,0$:
Set $A_n^+ = \{n+1, \ldots, N\}$.
If $c_i \geq c_m + c_r$:
Set $\hat{V}\left(n, x_j\right) = c_m$, $O(n,x_j) = 0$ for all j, and $\hat{\xi}_n = -\infty$. Proceed to the next epoch.
If $c_i + c_f > 0$ and $c_i < c_m + c_r$, compute $b_{n,N}$ and $\bar{b}_n$ using Theorem 1;
otherwise disable bound-based pruning.
For $j = 0,\ldots,M$, in increasing state order:
If the bounds certify $\bar{b}_n \leq x_j$
Set $\hat{V}(n, x_k) = c_m$ and $O(n,x_k) = 0$ for all $k \geq j$. Exit the state loop
Compute posterior parameters $\tilde{\mu}_{n,x_j}$ and $\tilde{\kappa}_n^2$ using Equation (3).
For every $a \in A_n^+$:
Obtain predictive mean m and standard deviation s from Equation (6)
Compute $R(n,x_j,a)$ using Equation (7).
Evaluate $\hat{I}_{n,x_j,a}$ using Equation (A3), and calculate the Equation (5) approximation:

$$\hat{Q}_a = c_i + \left(c_m + c_f\right)\left[1 - R\left(n, x_j, a\right)\right] + \hat{I}_{n,x_j,a}.$$

End the action loop
Set $C = \min_{a \in A_n^+} \hat{Q}_a$ and $a^* = \min\left\{a \in A_n^+ : \hat{Q}_a = C\right\}$.
If $C \geq c_m$:
Set $\hat{V}(n, x_k) = c_m$ and $O(n,x_k) = 0$ for all $k \geq j$. Exit the state loop.
Else
Set $\hat{V}\left(n, x_j\right) = C$ and $O(n,x_j) = a^*$.
End the state loop.
Record the first abort grid node and its preceding node as the switching bracket, if present.
End the epoch loop and return $\hat{V}$, O, and the threshold estimates or brackets.

Numerical implementation. The decision epochs are n = 0,...,N − 1, and the feasible continuation actions are $A_n^+ = \{n, +, 1 \ldots N\}$. The action a = Nrepresents continuation directly to mission completion. Each continuation action incurs one information-acquisition cost, including acquisition at the mission endpoint, consistently with Equation (5).

The theoretical nonfailed state space is $(-, \infty L)$. For computation, we introduce a lower boundary $x_{\min} < 0$ and a uniform grid $x_j = x_{\min} + j\Delta$, $j = 0, \ldots, M$, where $M\Delta = L - x_{\min}$. The endpoint $x_M = L$ is an auxiliary node storing the left-hand limit of the nonfailed value function, rather than the value of a failed state. Its value is obtained by evaluating the nonfailed recursion in the limit $x \uparrow L$. At the terminal epoch, all nonfailed grid values, including this auxiliary left-limit value, are initialized to $-c_r$. Actual states satisfying $x \geq L$ incur $c_m + c_f$, as specified in Equation (8).

For a subsequent epoch a, let $v_{a,j}$ denote the stored nonfailed value at node x_j. Between adjacent nodes, the value function is approximated by linear interpolation. Below $x_{\min}$, it is approximated by the constant $v_{a,0}$. Thus, the following applies:

$$\hat{V}_a(y) = \begin{cases} v_{a,0}, & y < x_{\min}, \\ [2mm] v_{a,j} + \frac{v_{a,j+1}-v_{a,j}}{\Delta}(y - x_j), & x_j \le y < x_{j+1},\ j = 0, \dots, M-1. \end{cases} \tag{30}$$

The probability of a transition below $x_{\min}$ is retained; the lower tail is neither discarded nor renormalized. The failure region $y \ge L$ is handled separately through its exact predictive probability, so interpolation does not smooth the failure boundary.

For a current state and continuation action, write the predictive distribution as $Y \sim \mathcal{N}(m, s^2)$, with m and s obtained from the posterior parameters in Equation (3). The following is defined:

$$z_j = \frac{x_j - m}{s}, \quad P_j = \Phi(z_{j+1}) - \Phi(z_j), \quad H_j = (m - x_j)P_j + s\Big[\phi(z_j) - \phi(z_{j+1})\Big]. \tag{31}$$

Here, Φ and ϕ are the standard normal cumulative distribution function and density. The integral of the interpolated value function is evaluated as follows:

$$\hat{I}_{n,x,a} = v_{a,0}\Phi(z_0) + \sum_{j=0}^{M-1}\left[v_{a,j}P_j + \frac{v_{a,j+1} - v_{a,j}}{\Delta}H_j\right]. \tag{32}$$

This expression integrates the piecewise linear approximation exactly under the Gaussian predictive distribution. The approximate continuation value is therefore $c_i + \big(c_m + c_f\big)[1 - R(n|x|a)] + \hat{I}_{n,x,a}$. For $a = N$, this reduces to the exact terminal action value $c_i + (c_m + c_f)[1 - R(n, x, N)] - c_r R(n, x, N)$.

At each epoch, states are processed in increasing order. Theorem 1 is used to assign analytically certified abort states without evaluating continuation actions. Otherwise, all feasible continuation actions are evaluated before applying the Bellman minimization. Once abort becomes optimal, higher grid states at the same epoch are assigned the abort action using state monotonicity. No assignments are propagated to other decision epochs. Ties between abort and continuation are resolved in favor of abort; ties between continuation actions are resolved by selecting the earliest acquisition epoch.

Backward induction terminates after epoch $n = 0$ has been processed. No iterative value-function convergence criterion is required for this finite-horizon recursion. Numerical accuracy is assessed separately by reducing Δ and extending the lower state boundary. The grid settings and the resulting changes in reported values and threshold locations are documented with the numerical experiments.

4. Numerical Experiment

To validate the efficacy of the proposed framework, we conduct numerical simulations targeting the driver of shipborne radar, which is an essential component responsible for the agile and precise orientation of the phased-array radar aboard maritime vessels. Operational integrity of the driver is fundamental to the radar's ability to fulfill its detection and tracking objectives under dynamic oceanic conditions. Given its pivotal role in orchestrating the mechanical motion of the array, its failure can compromise mission performance, pose safety hazards, and result in substantial material and strategic losses. Thus, proactive assessment and mitigation of degradation within radar drivers are critical for sustaining operational resilience throughout extended ocean expeditions. The degradation of radar drivers is influenced by a combination of mechanical fatigue, salinity-induced corrosion, and prolonged thermal cycling due to continuous exposure to harsh marine environments. Recent developments in embedded monitoring technologies, such as torque fluctuation

sensors and acoustic diagnostics, offer new opportunities for tracking the early progression of hidden defects.

This study emphasizes the role of mechanical vibration data in reflecting the evolving condition of the radar driver system. By analyzing some field performance degradation data of the driver, we found that collecting the mechanical vibration signals of the driver during operation and extracting characteristic values such as root mean square values as health indicators is a commonly used health diagnosis method. Due to its inherent non-stationary characteristics observed in real mission datasets, a non-monotonic stochastic process—specifically, a non-strictly monotonic stochastic process—is adopted to better represent the fluctuating nature of degradation over time. By analyzing mission-time vibration trajectories, the model captures the probabilistic evolution of damage, enabling prediction of failure likelihood with improved precision. Parameter estimation is grounded in actual degradation data sourced from long-term naval operations, and a series of simulation experiments are carried out to demonstrate the robustness and practical viability of the proposed prognostics-driven strategy.

4.1. Realization of the Optimal Policy

The numerical case is informed by vibration-monitoring records from ten radar drivers with recorded failures. The source records and platform-specific information are subject to confidentiality restrictions and are therefore not publicly released. The information used for modelling comprises observation times, vibration root-mean-square (RMS) indicators, and recorded failure status. The initial RMS level is subtracted from each trajectory to obtain a baseline-adjusted degradation indicator.

The random-effects Wiener model in Section 2 is fitted by marginal maximum likelihood, with the unit-specific drift integrated out under its Gaussian distribution. The parameters μ and κ describe the mean and between-unit variability of the drift, while σ describes within-unit stochastic fluctuations. For numerical presentation, a common positive scaling factor is applied to the degradation indicators across all units. The failure threshold and degradation parameters are transformed consistently to the same scale. The scaled parameters used in the numerical analysis are $\mu = 0.714$, $\kappa = 0.341$, and $\sigma = 0.09$. A mission with a duration of 20 days was selected for this case validation. During extended oceanic missions, in situ replacement or repair of the radar driver is not feasible without severely disrupting ongoing operations. Any attempt to intervene mid-mission would necessitate a full system halt, rendering the radar inoperative and jeopardizing the continuation of the mission. Given these constraints, the assessment of the radar driver's health status is limited to designated windows, typically scheduled at the end of each operational cycle—often once per 24-hour mission segment. Consequently, the minimum resolution for condition monitoring and fault detection is constrained to a daily interval. Thus, the unit time is set as $\delta = 1$. For ease of calculation, the costs of system failure and mission failure are quantified on an equal scale as $c_m = 3000$, $c_f = 5000$, $c_r = 4000$. Each time the driver is inspected and evaluated for its health condition, it will result in non-negligible time, equipment, and labor costs, which are denoted as $c_i = 200$.

Because the calibration sample contains only failed units, the fitted parameters may be affected by selection bias and should not be regarded as representative estimates for the entire operating population. The case therefore illustrates policy behavior under the specified degradation setting. A broader empirical calibration should incorporate surviving and right-censored units and account for the sampling mechanism.

Leveraging the above-mentioned data, we calculate the value function under the proposed policy and model. Figure 4 shows the overall trend of the value function across different decision epochs. This visual representation captures the relationship between the

system's degradation level and the associated optimal costs. In this numerical example, the computed value function decreases as the decision epoch advances at a fixed degradation level. This temporal trend is an observation under the specified parameter settings and is not asserted as a general structural property of the model.

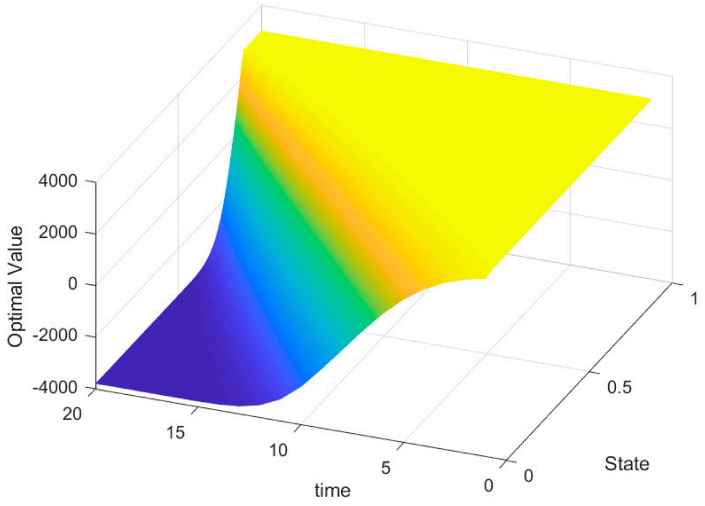


Figure 4. Optimal value function trend graph.

To observe the value function more clearly, we give a slice of the value function at a fixed epoch. Figure 5 presents a slice of the value function, showcasing how the expected cost of the system at a given time changes with the degree of degradation. The slice is consistent with Proposition 2, which establishes that the value function is non-decreasing in the degradation level at a fixed decision epoch.

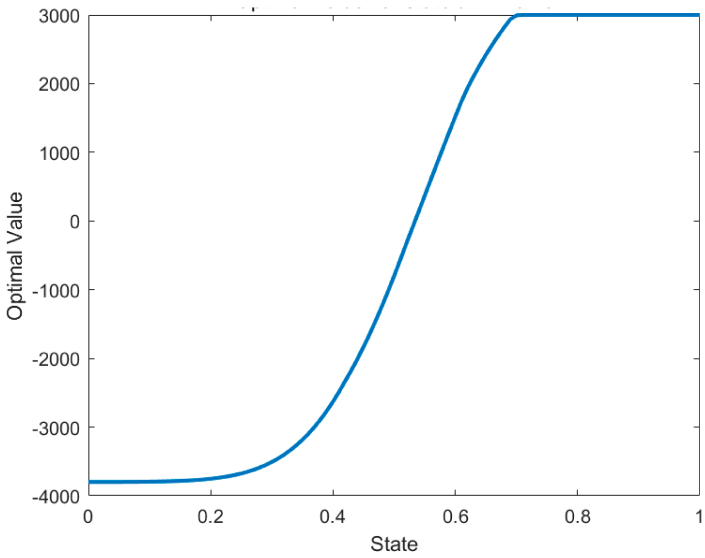


Figure 5. Trend slice of expected cost.

Figure 6 shows the change in the optimal inspection under different degradation levels. It shows that in the same epoch, the next optimal detection time is approaching with the increase in degradation level. That is, decision-makers are more inclined to arrange nearby detections to determine the degradation parameters and degradation level of the system in real time to ensure that correct decisions are made to avoid system failure. This also illustrates the validity of our model: non-periodic information acquisition is more conducive,

enabling decision-makers to rationally arrange detection and stop actions according to the level of system degradation.

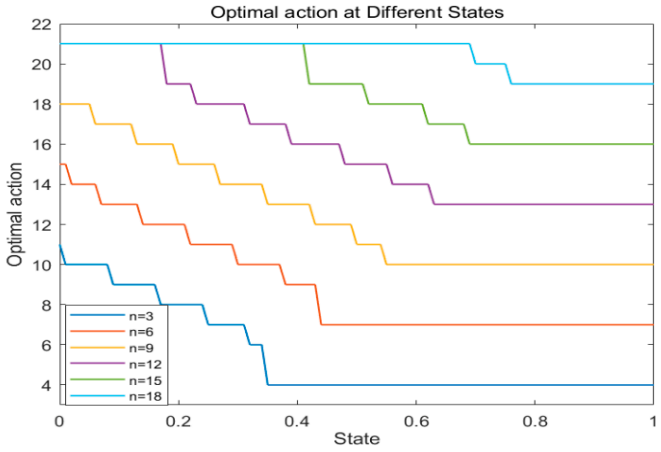


Figure 6. Optimal inspection action.

Figure 7 presents the computed mission-abort thresholds under different cost settings. For the parameter settings considered, the thresholds increase as the mission progresses, indicating that higher degradation levels are tolerated at later decision epochs. This temporal trend is specific to the numerical settings considered. Theorem 1 establishes the threshold structure and posterior-based bounds without imposing a general temporal ordering. The differences between the curves illustrate the influence of the cost parameters on mission-abort decisions.

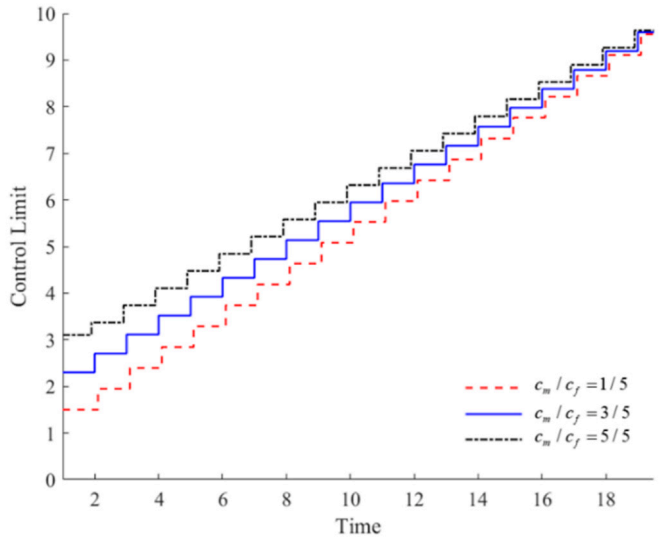


Figure 7. Control limit of different costs.

4.2. Policy Comparison

For comparison purposes, we present a series of heuristic policies that are commonly employed in mission abort models. The value functions under these comparative policies are established, and the comparative results are presented in the Numerical Experiment section.

Policy 1: Fixed inspection interval policy. The policy under consideration eliminates the decision optimization of detection intervals and replaces them with a fixed rhythm of information collection. At the same time, the method of parameter updating through the

collected information will not be cancelled. To this end, the value function is established as follows:

$$F(n,x) = \min\{F^0(n,x), F^1(n,x)\}, \tag{33}$$

Here, $F^0(n,x)$ and $F^1(n,x)$ represent the expected cost of aborting the mission and continuing the inspection at the next epoch, respectively.

Policy 2: Rigid policy without parameter learning. The policy considered still retains the characteristics of non-periodic information collection, but does not update the parameters based on real-time information. Therefore, the optimal decision equation is the same as in Equations (5) and (6); however, the reliability function and the state transition function do not account for parameter uncertainty. The comparison between this policy and the proposed policy can reflect the important role of parameter updating.

Policy 3: Benchmark policy without inspection adjustment and parameter learning. This policy is the most classic mission abort policy: it uses fixed monitoring of system health status information to decide whether to execute an abort, without considering parameter updates or non-periodic inspection means in the model framework. The comparison is to reflect the effectiveness of our improvement of the mission abort framework. Its Bellman equation can be referenced to Equation (16), but the kernel is not driven by the parameter-updating process.

To compare different policies, we selected the degradation trends of another 20 groups of radar drivers, conducted mission risk management for these simulations with the initial parameters and corresponding policies, and obtained the corresponding average costs shown in Tables 1 and 2. The economic superiority of the proposed strategy can be clearly seen from the results in the table. Among the three strategies, it is obvious that Policy 3 has the weakest performance. This is because it does not consider either parameter updates or irregular information acquisition, so it bears a higher failure risk and detection costs.

Table 1. Comparison of policies for different values of c_m with $c_f = 5000$\$.

	$c_m = 1000$		$c_m = 3000$		$c_m = 5000$	
	Cost	**Increase %**	**Cost**	**Increase %**	**Cost**	**Increase %**
Optimal policy	897	-	2322	-	3656	-
Policy 1	910	1.44	2521	8.57	3936	7.66
Policy 2	933	4.01	2601	12.01	4201	14.90
Policy 3	964	7.47	2862	23.25	4824	31.96

Table 2. Comparison of policies for different values of c_f with $c_m = 3000$\$.

	$c_f = 3000$		$c_f = 5000$		$c_f = 8000$	
	Cost	**Increase %**	**Cost**	**Increase %**	**Cost**	**Increase %**
Optimal policy	2193	-	2322	-	2693	-
Policy 1	2357	7.49	2521	8.57	2750	2.15
Policy 2	2524	15.12	2601	12.01	2809	4.31
Policy 3	2848	29.87	2862	23.25	2952	9.65

Tables 1 and 2 report the mean costs obtained for the limited set of radar-driver evaluation trajectories under the originally investigated settings. They indicate lower average costs for the proposed policy in that sample, but do not by themselves establish population-level

superiority. The following separately specified synthetic-path experiment provides additional outcome measures and a reproducible comparison under explicit model assumptions.

For a fair comparison of information-acquisition schedules in the supplementary simulation, the fixed-period policies are optimized ex ante over all integer inspection intervals $k = 1, \ldots, 20$ days, with an assessment at mission completion. The comparison results are shown in Table 3. Policy 1 retains Bayesian learning, whereas Policy 3 assumes a fixed drift $v = \mu$ without parameter updating. Policy 2 uses the same fixed-drift approximation while allowing adaptive acquisition. Under the specified simulation setting, the optimal fixed interval for Policy 1 is six days.

Table 3. Supplementary policy comparisons using 30,000 synthetic degradation trajectories.

Policy	Mean Cost	Success (%)	Failure (%)	Abort (%)	Mean Acquisitions
Proposed	1461.3	26.24	0.46	73.3	1.38
Policy 1	1570.5	26.2	0.66	73.14	1.86
Policy 2	2891.4	0	0	96.7	1.01
Policy 3	3000.0	0	0	100	0

The finite-horizon backward induction algorithm is implemented on a uniform degradation-state grid over $[-12, 10]$, with grid spacing $\Delta = 0.1$. The Gaussian expectation of the piecewise-linear continuation value is evaluated analytically, while the probability of entering the failure region is treated separately. The computed initial expected costs of the proposed and optimized fixed-period learning policies are 1450.4 and 1563.5, respectively. Reducing Δ to 0.05 changes these values to 1450.2 and 1563.2. Extending the lower state boundary to -20 produces no change at the reported precision. Compared with the optimized fixed-period learning policy, the proposed policy reduces simulated mean cost by 109.1 units, corresponding to a reduction of 6.95%. The proposed policy also produces a lower inspection-epoch failure probability and requires fewer information acquisitions on average. These findings illustrate the potential benefits of joint acquisition and abort optimization under the stated assumptions.

5. Conclusions

This paper develops a mission risk management framework that jointly determines adaptive information-acquisition and mission-abort decisions while updating uncertainty in a unit-specific degradation drift. Under the specified model and observation assumptions, the latest observation and its acquisition time are sufficient for posterior updating. The structural analysis characterizes the abort region, provides posterior-based threshold bounds, and establishes the relationship between acquisition cost and optimal expected acquisition effort. These results support the development of an efficient backward induction algorithm. The numerical study illustrates the potential economic benefits of the framework under the investigated settings. These observations depend on the adopted inspection-epoch failure criterion, selected cost parameters, and limited set of evaluation trajectories. The costs are illustrative rather than empirically validated estimates of operational losses, and calibration based only on failed units may introduce selection bias. Accordingly, the results provide preliminary evidence of potential effectiveness. Broader practical applicability requires further validation using representative degradation data and application-specific cost estimates.

Future research can build upon the framework developed in this study by exploring several promising directions. First, extending the mission abort framework to consider multiple uncertainties, such as environmental factors and operational variations, could

provide a more robust decision-making model that accounts for the complexities of real-world systems. Second, investigating the detection and maintenance (or abort) strategies for individual components in complex systems would enhance the framework's adaptability and effectiveness, particularly in multi-component systems where component-specific degradation and failure risks vary. Lastly, integrating constraints such as resource availability, time limitations, and operational capacity into the mission abort decision framework would offer a more comprehensive approach to mission risk management, optimizing both mission outcomes and resource usage in scenarios with multiple operational constraints. These advancements would further improve the flexibility and applicability of mission abort strategies across diverse critical systems and environments.

Author Contributions: Conceptualization, F.W.; Methodology, F.W.; Software, F.W.; Validation, F.W.; Formal Analysis, F.W.; Data Curation, S.Z.; Writing—Review and Editing, Y.C. and S.Z.; Visualization, Y.C. All authors have read and agreed to the published version of the manuscript.

Funding: This research received no external funding.

Data Availability Statement: The original contributions presented in this study are included in the article. Further inquiries can be directed to the corresponding author.

Conflicts of Interest: The authors declare no conflict of interest.

References

1. Levitin, G.; Finkelstein, M.; Huang, H. Optimal mission abort policies for multistate systems. *Reliab. Eng. Syst. Saf.* **2020**, *193*, 106671. [CrossRef]
2. Peng, R.; Zhai, Q.; Xing, L.; Yang, J. Reliability analysis and optimal structure of series-parallel phased-mission systems subject to fault-level coverage. *IISE Trans.* **2016**, *48*, 736–746. [CrossRef]
3. Jardine, A.; Lin, D.; Banjevic, D. A review on machinery diagnostics and prognostics implementing condition-based maintenance. *Mech. Syst. Signal Process.* **2006**, *20*, 1483–1510. [CrossRef]
4. Bucolo, M.; Fortuna, L.; La Rosa, M. Complex dynamics through fuzzy chains. *IEEE Trans. Fuzzy Syst.* **2004**, *12*, 289–295. [CrossRef]
5. Yang, L.; Zhang, X.; Zhu, F.; Wang, Z.; Zhang, X. Semi-supervised Cross-domain Fault Diagnosis via Contrastive Pre-training and Annotation-efficient Alignment Strategy. *J. Ind. Inf. Integr.* **2026**, *50*, 101076. [CrossRef]
6. Xiao, H.; Zhang, Y.; Xiang, Y.; Peng, R. Optimal design of a linear sliding window system with consideration of performance sharing. *Reliab. Eng. Syst. Saf.* **2020**, *198*, 106900. [CrossRef]
7. Wang, N.; Tian, T.; Yang, L.; Zhang, C.; Liu, L.; Yang, J. Timely reliability evaluation and optimization of wireless sensor networks considering channel capacity randomness and energy depletion. *IEEE Internet Things J.* **2026**, *13*, 33065–33083. [CrossRef]
8. Yang, L.; Wang, J.; Xie, M. Graph-based reliability evaluation of a reconfigurable multi-stage system using sequential unconnected path sets. *Reliab. Eng. Syst. Saf.* **2025**, *261*, 111093. [CrossRef]
9. Zhou, S.; Yang, L.; Yang, L.; Ma, X. A self-adaptive group maintenance policy for multi-state systems under postponed replacement: A state-action interaction approach. *Reliab. Eng. Syst. Saf.* **2027**, *277*, 112921. [CrossRef]
10. Myers, A. Probability of loss assessment of critical k-out-of-n: G systems having a mission abort policy. *IEEE Trans. Reliab.* **2009**, *58*, 694–701. [CrossRef]
11. Wang, J.; Tang, L.; Ma, X.; Gao, K.; Jia, H.; Yang, L. Prognosis-driven reliability analysis and replacement policy optimization for two-phase continuous degradation. *Reliab. Eng. Syst. Saf.* **2023**, *230*, 108909. [CrossRef]
12. Yang, L.; Ma, X.; Peng, R.; Zhai, Q.; Zhao, Y. A preventive maintenance policy based on dependent two-stage deterioration and external shocks. *Reliab. Eng. Syst. Saf.* **2017**, *160*, 201–211. [CrossRef]
13. Wang, J.; Ma, X.; Qiu, Q.; Shang, L.; Wang, J. A hybrid inspection-replacement policy for multi-stage degradation considering imperfect inspection with variable probabilities. *Reliab. Eng. Syst. Saf.* **2023**, *241*, 109629. [CrossRef]
14. Wang, J.; Peng, R.; Qiu, Q.; Yang, L. An inspection-based replacement planning in consideration of state-driven imperfect inspections. *Reliab. Eng. Syst. Saf.* **2023**, *232*, 109064. [CrossRef]
15. Ji, Z.; Chen, Y.; Ma, X.; Cai, Y.; Yang, L. Hierarchical condition-based maintenance planning for corrosion process considering natural environmental impact. *Reliab. Eng. Syst. Saf.* **2024**, *243*, 109856. [CrossRef]
16. Ma, X.; Han, R.; Chen, Y.; Qiu, Q.; Yan, R.; Yang, L. Intelligent spare ordering and replacement optimisation leveraging adaptive prediction information. *Reliab. Eng. Syst. Saf.* **2024**, *252*, 110420. [CrossRef]

17. Jia, H.; Peng, R.; Yang, L.; Wu, T.; Liu, D.; Li, Y. Reliability evaluation of demand-based warm standby systems with capacity storage. *Reliab. Eng. Syst. Saf.* **2022**, *218*, 108132. [CrossRef]
18. Wang, J.; Yang, L.; Ma, X.; Peng, R. Joint optimization of multi-window maintenance and spare part provisioning policies for production systems. *Reliab. Eng. Syst. Saf.* **2021**, *216*, 108006. [CrossRef]
19. Zhang, Z.; Yang, L. Postponed maintenance scheduling integrating state variation and environmental impact. *Reliab. Eng. Syst. Saf.* **2020**, *202*, 107065. [CrossRef]
20. Ma, X.; Liu, B.; Yang, L.; Peng, R.; Zhang, X. Reliability analysis and condition-based maintenance optimization for a warm standby cooling system. *Reliab. Eng. Syst. Saf.* **2020**, *193*, 106588. [CrossRef]
21. Shang, L.; Liu, B.; Qiu, Q.; Yang, L. Three-dimensional warranty and post-warranty maintenance of products with monitored mission cycles. *Reliab. Eng. Syst. Saf.* **2023**, *239*, 109506. [CrossRef]
22. Wang, J.; Ma, X.; Gao, K.; Zhao, Y.; Yang, L. Condition-based maintenance management for two-stage continuous deterioration with two-dimensional inspection errors. *Qual. Reliab. Eng. Int.* **2024**, *40*, 3691–3708. [CrossRef]
23. Yang, L.; Zhao, Y.; Ma, X. An inspection model for a multi-component system subject to 2 types of failures. *Qual. Reliab. Eng. Int.* **2017**, *33*, 2539–2549. [CrossRef]
24. Yang, L.; Zhao, Y.; Ma, X.; Qiu, Q. An optimal inspection and replacement policy for a two-unit system. *Proc. Inst. Mech. Eng. Part O J. Risk Reliab.* **2018**, *232*, 766–776. [CrossRef]
25. Wu, D.; Gao, K.; Peng, R.; Sun, J.; Yang, L.; Wei, F. Optimal Preventive Maintenance Policy Considering Technical-Innovation-Empowered Renewals. *Proc. Inst. Mech. Eng. Part O J. Risk Reliab.* **2026**, *240*, 1103–1119. [CrossRef]
26. Wang, J.; Ma, X.; Yang, L. Hybrid maintenance optimization for multi-state competing failure systems under inspection uncertainties and spare dynamics. *Reliab. Eng. Syst. Saf.* **2026**, *272*, 112524. [CrossRef]
27. Zhou, S.; Ma, X.; Wang, J.; Chen, Y.; Yang, L. Global-dynamic maintenance management of multi-component degrading plants with non-immediate replacement: A self-adaptive grouping approach. *Maint. Reliab. I Niezawodn.* **2025**, *27*, 1–19. [CrossRef]
28. Wang, J.; Ma, X.; Zhao, Y.; Yang, L. A condition-based maintenance policy for two-stage continuous degradation considering inspection errors. In Proceedings of the 2023 5th International Conference on System Reliability and Safety Engineering (SRSE), Beijing, China, 20–23 October 2023; pp. 339–346.
29. Wang, J.; Fu, Y.; Zhou, J.; Yang, L.; Yang, Y. Condition-based maintenance for redundant systems considering spare inventory with stochastic lead time. *Reliab. Eng. Syst. Saf.* **2025**, *257*, 110837. [CrossRef]
30. Qiu, Q.; Cui, L. Gamma process based optimal mission abort policy. *Reliab. Eng. Syst. Saf.* **2019**, *190*, 106496. [CrossRef]
31. Peng, R.; Zhai, Q.; Xing, L.; Yang, J. Reliability of demand-based phased-mission systems subject to fault level coverage. *Reliab. Eng. Syst. Saf.* **2014**, *121*, 18–25. [CrossRef]
32. Qiu, Q.; Maillart, L.; Prokopyev, O.; Cui, L. Optimal condition-based mission abort decisions. *IEEE Trans. Reliab.* **2022**, *72*, 408–425. [CrossRef]
33. Yang, L. An evidence-based likelihood approach for the reliability of a complex system with overlapped failure data. *Comput. Ind. Eng.* **2025**, *201*, 110893. [CrossRef]
34. Wang, J.; Zhao, Y.; Liu, C.; Li, S.; Zhang, R.; Zhan, J.; Ji, H. Predictive Opportunistic Maintenance for k-out-of-n Systems with Heterogeneous Two-Stage Degradation. *Mathematics* **2026**, *14*, 3334. [CrossRef]
35. Yang, L.; Chen, Y.; Ma, X.; Qiu, Q.; Peng, R. A Prognosis-centered Intelligent Maintenance Optimization Framework under Uncertain Failure Threshold. *IEEE Trans. Reliab.* **2024**, *73*, 115–130. [CrossRef]
36. Yang, L.; Sun, Q.; Ye, Z.S. Designing mission abort strategies based on early-warning information: Application to UAV. *IEEE Trans. Ind. Inform.* **2019**, *16*, 277–287. [CrossRef]
37. De Jonge, B.; Scarf, P.A. A review on maintenance optimization. *Eur. J. Oper. Res.* **2020**, *285*, 805–824. [CrossRef]
38. Zhao, X.; Sun, J.; Qiu, Q.; Chen, K. Optimal inspection and mission abort policies for systems subject to degradation. *Eur. J. Oper. Res.* **2021**, *292*, 610–621. [CrossRef]
39. Yang, L.; Chen, Y.; Qiu, Q.; Wang, J. Risk control of mission-critical systems: Abort decision-makings integrating health and age conditions. *IEEE Trans. Ind. Inform.* **2022**, *18*, 6887–6894. [CrossRef]
40. Cheng, G.; Li, L.; Shangguan, C. Optimal joint inspection and mission abort policy for a partially observable system. *Reliab. Eng. Syst. Saf.* **2022**, *229*, 108870. [CrossRef]
41. Yang, L.; Wei, F.; Qiu, Q. Mission risk control via joint optimization of sampling and abort decisions. *Risk Anal.* **2024**, *44*, 666–685. [CrossRef]
42. Levitin, G.; Xing, L.; Dai, Y. Mission abort policy in heterogeneous nonrepairable 1-out-of-N warm standby systems. *IEEE Trans. Reliab.* **2017**, *67*, 342–354. [CrossRef]
43. Peng, R. Joint routing and aborting optimization of cooperative unmanned aerial vehicles. *Reliab. Eng. Syst. Saf.* **2018**, *177*, 131–137. [CrossRef]
44. Yang, L.; Ma, X.; Zhai, Q.; Zhao, Y. A delay time model for a mission-based system subject to periodic and random inspection and postponed replacement. *Reliab. Eng. Syst. Saf.* **2016**, *150*, 96–104. [CrossRef]

45. Levitin, G.; Xing, L.; Dai, Y. Mission abort policy for systems with observable states of standby components. *Risk Anal.* **2020**, *40*, 1900–1912. [CrossRef]
46. Levitin, G.; Finkelstein, M.; Xiang, Y. Optimal mission abort policies for repairable multistate systems performing multi-attempt mission. *Reliab. Eng. Syst. Saf.* **2021**, *209*, 107497. [CrossRef]
47. Xing, L. Reliability evaluation of phased-mission systems with imperfect fault coverage and common-cause failures. *IEEE Trans. Reliab.* **2007**, *56*, 58–68. [CrossRef]
48. Wang, L.; Li, B.; Zhao, X. Multi-objective predictive maintenance scheduling models integrating remaining useful life prediction and maintenance decisions. *Comput. Ind. Eng.* **2024**, *197*, 110581. [CrossRef]
49. Wang, J.; Ma, X.; Zhao, Y.; Ma, X.; Xiao, H.; Ma, Y.; Peng, R.; Yang, L. A State-Age-Dependent Maintenance-Spare Control Strategy under Inspection Error Compensation. *IEEE Trans. Reliab.* **2025**, *74*, 5805–5819. [CrossRef]
50. Yang, L.; Zhao, Y.; Peng, R.; Ma, X. Hybrid preventive maintenance of competing failures under random environment. *Reliab. Eng. Syst. Saf.* **2018**, *174*, 130–140. [CrossRef]
51. Peng, R.; He, X.; Zhong, C.; Kou, G.; Xiao, H. Preventive maintenance for heterogeneous parallel systems with two failure modes. *Reliab. Eng. Syst. Saf.* **2022**, *220*, 108310. [CrossRef]
52. Yang, L.; Zhang, X.; Lu, Z.; Fu, Y.; Moens, D.; Beer, M. Reliability evaluation of a multi-state system with dependent components and imprecise parameters: A structural reliability treatment. *Reliab. Eng. Syst. Saf.* **2024**, *250*, 110240. [CrossRef]
53. Levitin, G.; Xing, L.; Dai, Y. Optimal scheduling, loading and aborting in additive missions performed by multiple components in shock environment. *Reliab. Eng. Syst. Saf.* **2025**, *256*, 110750. [CrossRef]
54. Siegmund, D. *Sequential Analysis: Tests and Confidence Intervals*; Springer: Berlin/Heidelberg, Germany, 1985.
55. Shiryaev, A.N. *Optimal Stopping Rules*; Springer: Berlin/Heidelberg, Germany, 2008.
56. Liu, B.; Wu, S.; Xie, M.; Kuo, W. A condition-based maintenance policy for degrading systems with age- and state-dependent operating cost. *Eur. J. Oper. Res.* **2017**, *263*, 879–887. [CrossRef]

Disclaimer/Publisher's Note: The statements, opinions and data contained in all publications are solely those of the individual author(s) and contributor(s) and not of MDPI and/or the editor(s). MDPI and/or the editor(s) disclaim responsibility for any injury to people or property resulting from any ideas, methods, instructions or products referred to in the content.